SF2A 2010
S. Boissier, M. Heydari-Malayeri, R. Samadi and D. Valls-Gabaud (eds)

THERMOHALINE INSTABILITY AND ROTATION-INDUCED MIXING IN LOW- AND INTERMEDIATE-MASS STARS

N. Lagarde[1] and C. Charbonnel [1, 2]

Abstract. Thermohaline mixing was recently identified as the dominating process that governs the photospheric composition of low-mass bright giant stars (Charbonnel & Zahn 2007a). Here we present the predictions of our stellar models computed with the code STAREVOL, taking into account this mechanism together with rotational mixing. We compare the predictions for the surface abundances with recent observations in evolved stars, and discuss the corresponding ^{3}He yields in the context of Galactic chemical evolution.

Keywords: hydrodynamics, instabilities, stars: abundances, evolution, rotation, Galaxy: abundances

1 Introduction

At all stages of their evolution, low- and intermediate-mass stars (LIMS) exhibit the signatures of complex physical processes that require challenging modelling beyond canonical (or standard) stellar theory (by canonical we refer to the modelling of non-rotating, non-magnetic stars, in which convection is the only mechanism that drives mixing in stellar interiors). Charbonnel & Zahn (2007, hereafter CZ07) identified thermohaline mixing as the process that governs the surface abundances of LIMS evolving on the upper end of the red giant branch (RGB). In these stars, this double-diffusive instability is induced by the mean molecular weight inversion created by the $^3He(^3He, 2p)^4He$ reaction in the radiative layers between the convective envelope and the hydrogen burning shell (Eggleton et al. 2006). Here we focuss on the case of LIMS of solar-metallicity. We discuss the cumulated impact of thermohaline and rotation-induced mixings on the surface abundances, based on models computed with the code STAREVOL (see e.g. Decressin et al. 2009). Details on the assumptions and computations can be found in Charbonnel & Lagarde (2010), together with a more complete comparison with observations in Galactic open clusters.

2 Models and results

In order to quantify precisely the impact of each transport process at the various evolutionary phases, we have computed models with the following assumptions: (1) Standard models (no mixing mechanism other than convection); (2) Models including thermohaline mixing only (rotation velocity V=0); (3) Models including thermohaline mixing and rotation-induced processes for different initial rotation velocities.

For the turbulent diffusivity produced by the thermohaline instablity, we use the prescription advocated by CZ07 based on Ulrich (1972) arguments for the aspect ratio α (length/width) of the salt fingers as supported by laboratory experiments (Krishnamurti 2003) and including Kippenhahn et al. (1980) extended expression for the case of a non-perfect gas. For the treatment of rotation-induced mixing we proceed as follows. Solid-body rotation is assumed when the star arrives on the zero age main sequence (ZAMS). Typical initial (i.e., ZAMS) rotation velocities are chosen depending on the stellar mass based on observed rotation distributions in young open clusters (Gaigé 1993). Surface braking by a magnetic torque is applied for stars with an effective temperature on the ZAMS lower than 6900 K that have relatively a thick convective envelope as discussed in Talon & Charbonnel (1998); the adopted braking law follows the description of Kawaler (1988). From the ZAMS on, the evolution of the internal angular momentum profile is accounted for with the complete formalism developed by Zahn (1992) and Maeder & Zahn (1998) that takes into account advection by meridional circulation and diffusion by shear turbulence.

[1] Geneva Observatory, University of Geneva, Chemin des Maillettes 51, 1290 Versoix, Switzerland
[2] LATT, CNRS UMR 5572, Toulouse University, 14, av. E.Belin, 31400 Toulouse, France

2.1 Models predictions for $^{12}C/^{13}C$

In figure 1, we present observations of carbon isotopic ratio in evolved stars belonging to different Galactic open clusters, as a function of cluster's turn off mass. The data are compared with our theoritical predictions at solar metallicity. For low-mass stars ($M < 1.7M_{\odot}$), thermohaline mixing on the RGB appears to be the main mecanism explaining the low-carbon isotopic ratios observed. On the other hand, rotation-induced mixing is found to change the stellar structure so that in the mass range between $\sim$ 1.5 and 2.2 $M_{\odot}$ the thermohaline instability occurs earlier on the red giant branch than in non-rotating models. Finally, rotation accounts for the observed star-to-star abundance variations at a given evolutionary status, and is necessary to explain the features of CN-processed material in intermediate-mass stars.

2.2 Models predictions for Lithium on TP-AGB

In all the models that we have computed along the TP-AGB, thermohaline transport leads to non negligible fresh lithium production, as shown in figure 2. There we present the evolution of the surface lithium abundance N(Li) as a function of effective temperature and bolometric magnitude for TP-AGB models of 1.25 and 2.0$M_{\odot}$ stars. Theoritical predictions are compared with observations in the sample of low-mass oxygen-rich AGB variables belonging to the Galactic disk studied by Uttenthaler & Lebzelter (2010). Let us note that despite this strong Li production at that phase, the total stellar Li yields remain negative.

2.3 Models predictions for ^{3}He

In figure 3, we present the evolution of ^{3}He mass fraction at the surface of 1$M_{\odot}$ model at solar metallicity in the standard case and in the case with thermohaline mixing (black solid and red dotted lines respectively). Thermohaline mixing induces a strong decrease of ^{3}He at the bump luminosity, and the mass fraction of ^{3}He at the AGB tip is strongly reduced when thermohaline mixing is accounted for compared to the standard predictions. As a consequence, the overal ^{3}He yields are also strongly affected, as shown in 4. As will be discussed elsewhere (Lagarde et al., in preparation), this helps reconciling the theoretical Galactic evolution of ^{3}He with observations of this element in Galactic HII regions (i.e Balser et al. 1994, 1999; Bania et al. 1997, 2002).

3 Conclusions

An inversion of molecular weight created by the $^{3}He(^{3}He, 2p)^{4}He$ reaction is at the origin of thermohaline mixing in low- and intermediate-mass stars brighter than the luminosity of the bump on the RGB (see e.g. CZ07). Models including the transport of chemical induced by this double-diffusive instability explain very well the observations of ^{12}C/^{13}C in low-mass stars in Galactic open clusters. Rotation-induced mixing allows us to explain the ^{12}C/^{13}C anomalies in giant stars with a mass higher than $1.7M_{\odot}$. Thermohaline mixing has also an effect during TP-AGB, where it allows the production of lithium, in agreement with observations in oxygen-rich variables. Finaly, it can help reconciling the theoretical ^{3}He yields with the behaviour of this primordial element in the Galaxy.

References

Balser, D. S., Bania, T. M., Brockway, C. J., Rood, R. T., & Wilson, T. L. 1994, ApJ, 430, 667
Balser, D. S., Bania, T. M., Rood, R. T., & Wilson, T. L. 1999, ApJ, 510, 759
Bania, T. M., Balser, D. S., Rood, R. T., Wilson, T. L., & Wilson, T. J. 1997, ApJS, 113, 353
Bania, T. M., Rood, R. T., & Balser, D. S. 2002, Nature, 415, 54
Charbonnel, C. & Lagarde, N. 2010, ArXiv e-prints
Charbonnel, C. & Zahn, J.-P. 2007, A&A, 467, L15
Decressin, T., Mathis, S., Palacios, A., et al. 2009, A&A , 495, 271
Eggleton, P. P., Dearborn, D. S. P., & Lattanzio, J. C. 2006, Science, 314, 1580
Gaigé, Y. 1993, A&A, 269, 267
Gilroy, K. K. 1989, ApJ, 347, 835

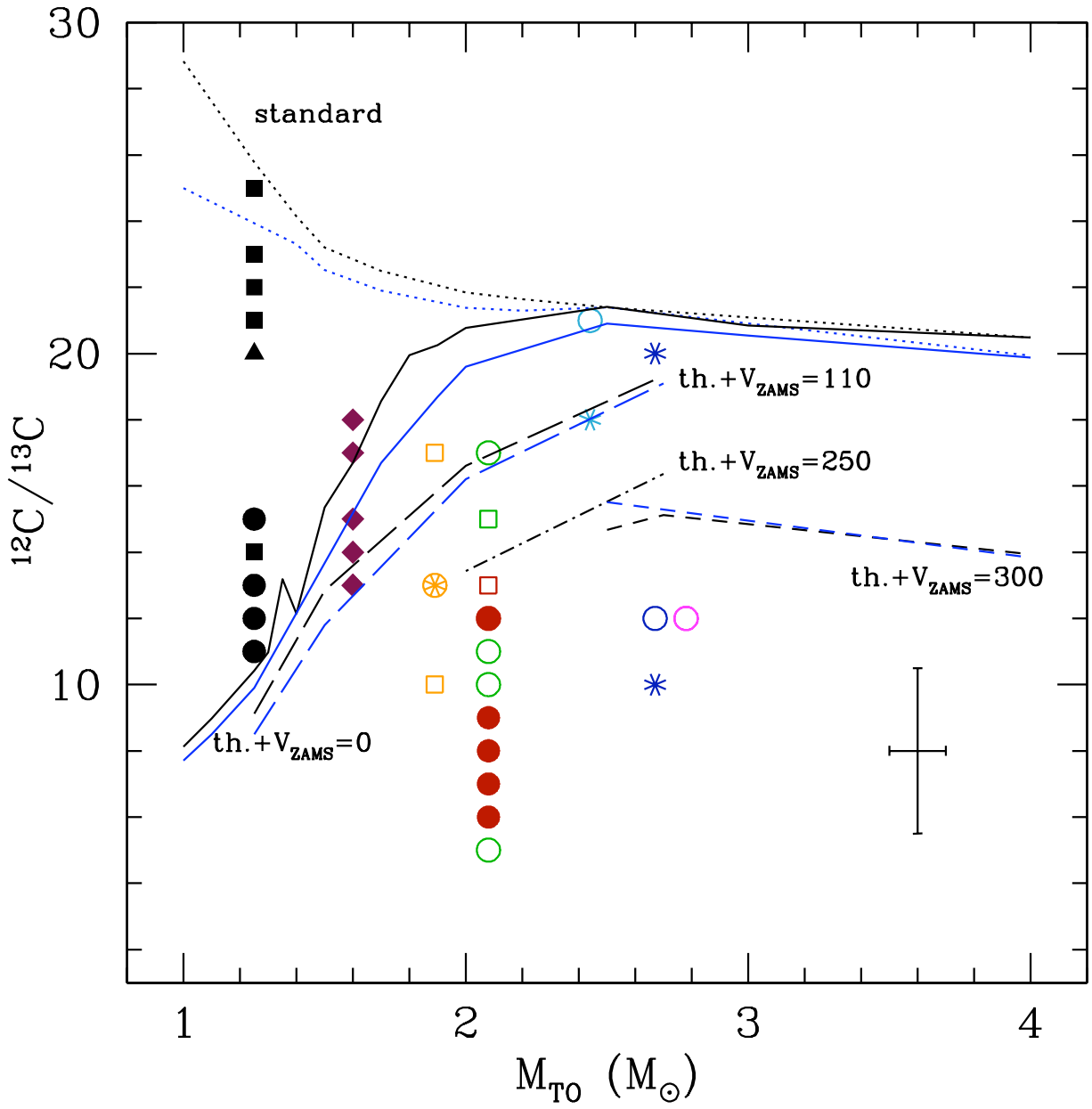

Fig. 1. Observations of $^{12}C/^{13}C$ in evolved stars of Galactic open clusters by Smiljanic et al. (2009, open cluster), Gilroy (1989), Gilroy & Brown (1991), and Mikolaitis et al. (2010) as a function of the turnoff mass of the corresponding host cluster. Squares, circles, and asteriscs are for RGB, clump, and early-AGB stars respectively, while diamonds are for stars from Gilroy (1989) sample with doubtful evolutionary status; triangles are for lower limits. A typical error bar is indicated. Theoretical predictions are shown at the tip of the RGB and after completion of the second dredge-up (black and blue lines respectively). Standard models (no thermohaline nor rotation-induced mixing) are shown as dotted lines, models with thermohaline mixing only (V_{ZAMS}=0) as solid lines, and models with thermohaline and rotation-induced mixing for different initial rotation velocities as indicated as long-dashed, dot-dashed, and dashed lines. Figure from Charbonnel & Lagarde (2010).

Gilroy, K. K. & Brown, J. A. 1991, ApJ, 371, 578

Kawaler, S. D. 1988, ApJ, 333, 236

Kippenhahn, R., Ruschenplatt, G., & Thomas, H.-C. 1980, A&A, 91, 175

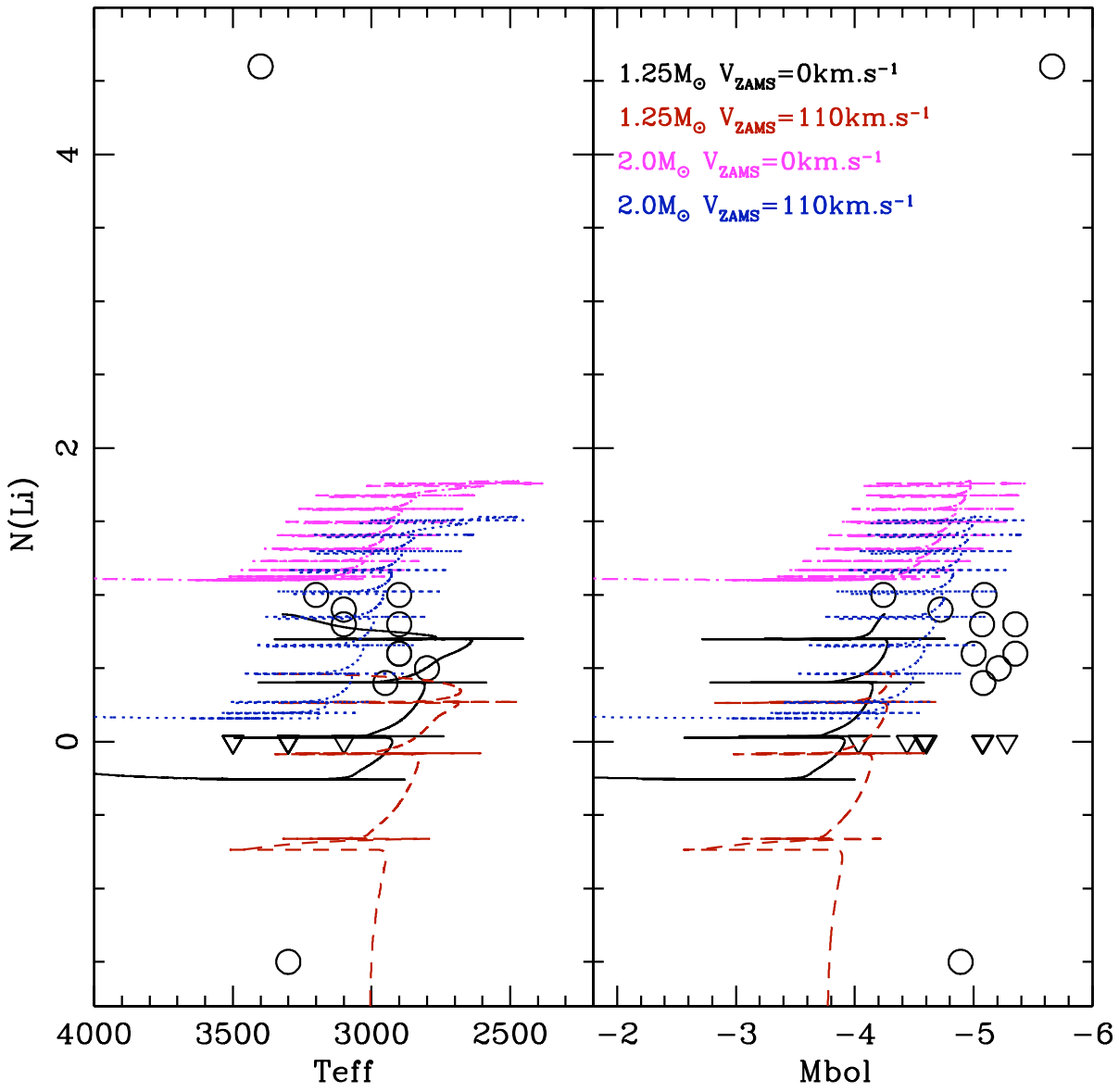

Fig. 2. Lithium observations in oxygen-rich variables belonging to the Galactic disk (Uttenthaler & Lebzelter 2010); circles and triangles are for abundance determinations and upper limits respectively) as a function of effective temperature and bolometric magnitude. Theoretical lithium evolution is shown from the early-AGB up to the end of the TP-AGB. Various lines correspond to predictions for stellar models of different masses computed without or with rotation as indicated, and with thermohaline mixing in all cases. Figure from Charbonnel & Lagarde (2010).

Krishnamurti, R. 2003, Journal of Fluid Mechanics, 483, 287
Maeder, A. & Zahn, J.-P. 1998, A&A, 334, 1000
Mikolaitis, Š., Tautvaišienė, G., Gratton, R., Bragaglia, A., & Carretta, E. 2010, MNRAS, 407, 1866
Smiljanic, R., Gauderon, R., North, P., et al. 2009, A&A, 502, 267
Talon, S. & Charbonnel, C. 1998, A&A, 335, 959
Ulrich, R. K. 1972, ApJ, 172, 165
Uttenthaler, S. & Lebzelter, T. 2010, A&A, 510, A62+

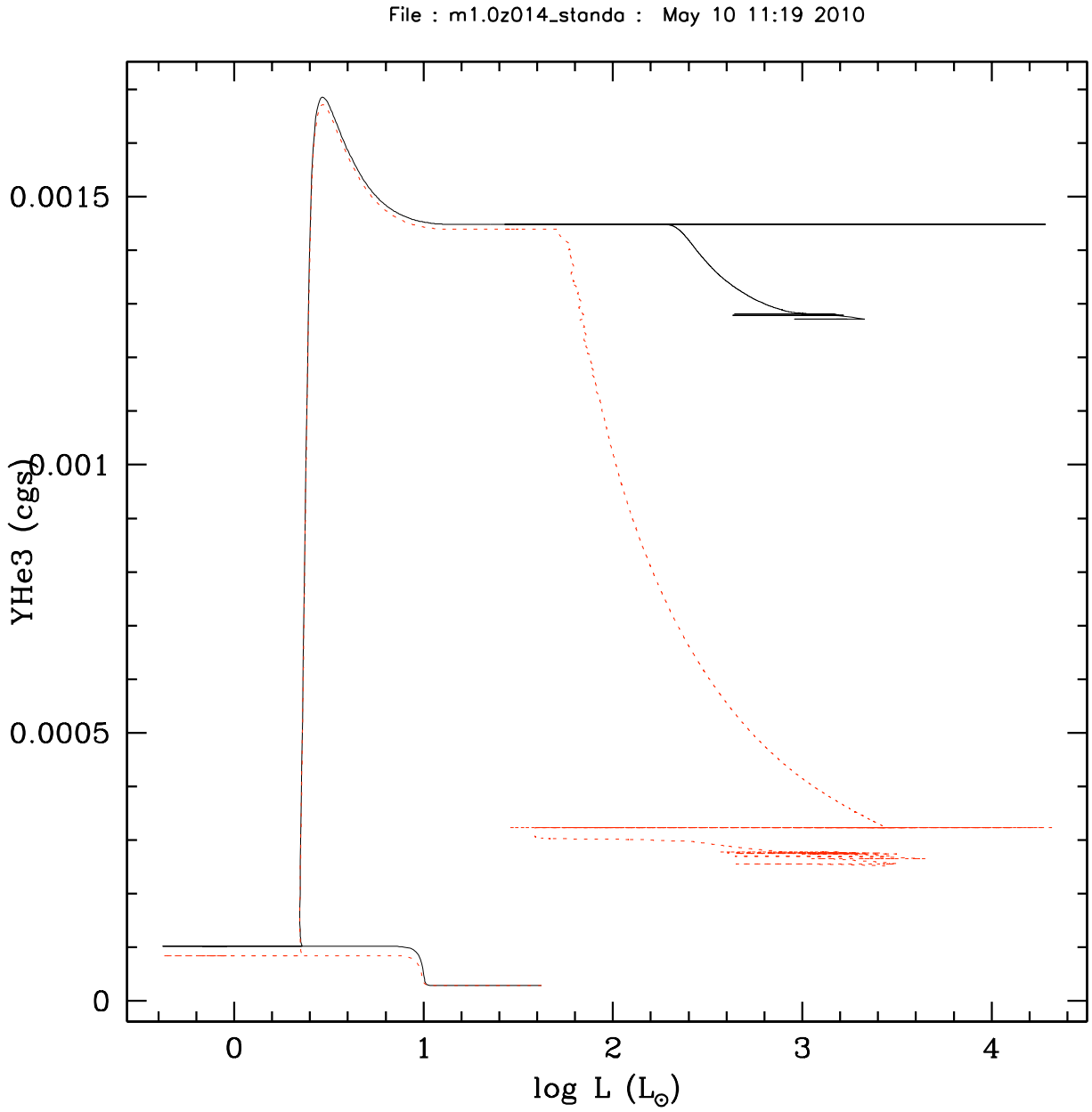

Fig. 3. Evolution of the surface abundance of ^{3}He (in mass fraction) from the pre-main sequence up to the AGB tip for $1M_\odot$ models at solar metallicity. The black solid line and the red dotted-line correspond to the standard and thermohaline cases respectively.

Zahn, J.-P. 1992, A&A, 265, 115

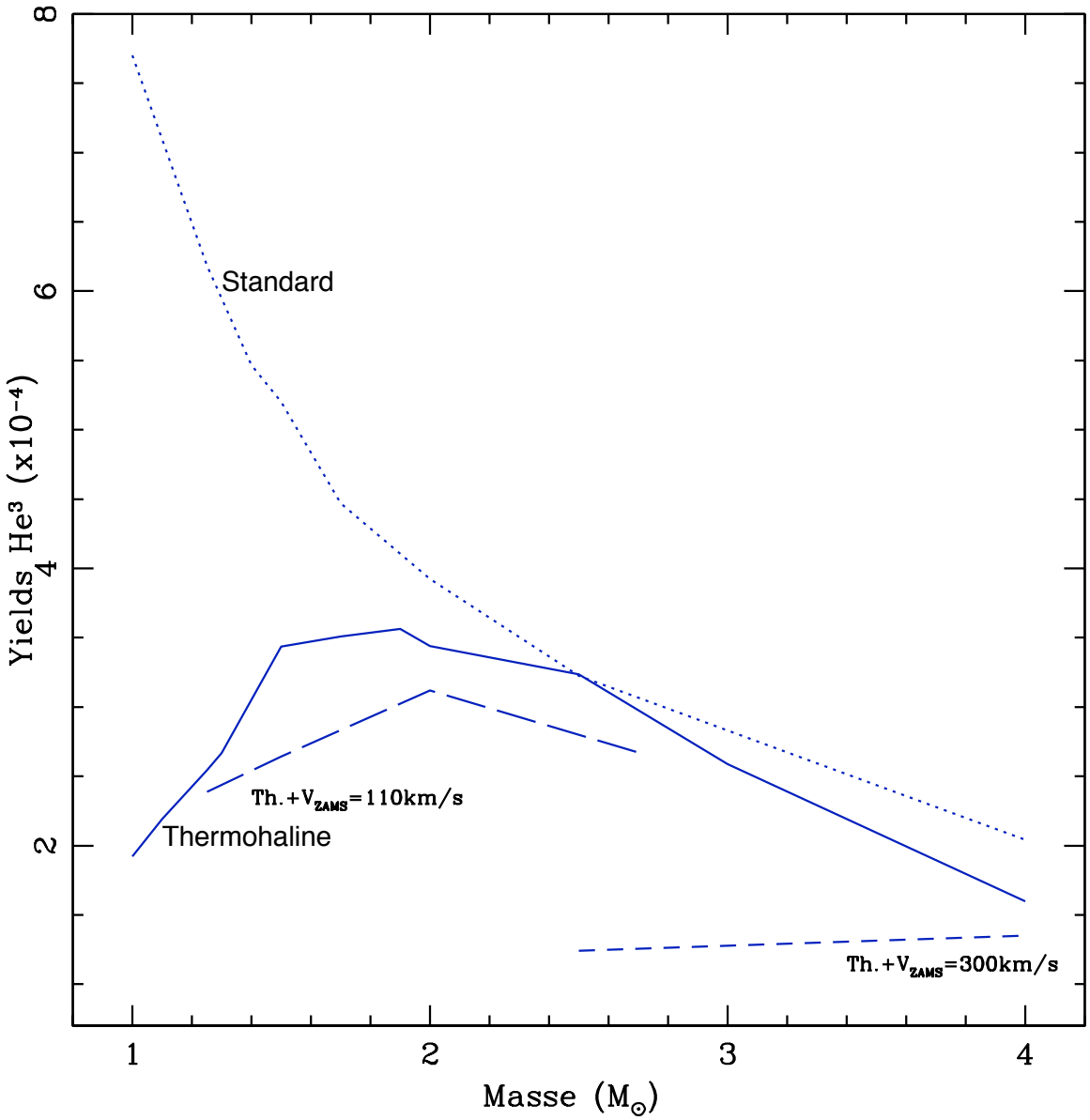

Fig. 4. Theoretical ^{3}He yields at solar metallicity as a function of initial stellar mass. The standard predictitions are shown by the dotted line; the thermohaline predictions are shown by the solid line; and the rotation+thermohaline models are shown as a long dashed lines for $V_{ZAMS} = 110km/s$ and as a short dashed lines for $V_{ZAMS} = 300km/s$. Figure from Lagarde et al. (in prep.)